

An NMR Study of Translational Diffusion and Structural Anisotropy in Magnetically Alignable Nonionic Surfactant Mesophases

Anand Yethiraj,^{*,†} Donatella Capitani,[‡] Nicholas E. Burlinson,[†] and E. Elliott Burnell[†]

Chemistry Department, University of British Columbia, 2036 Main Mall, Vancouver, B.C. V6T 1Z1, Canada, and Institute of Chemical Methodologies, CNR, Research Area of Rome, Via Salaria Km 29-300, Monterotondo Staz, Rome, Italy

Received December 10, 2004. In Final Form: January 25, 2005

The diffusion of both water and surfactant components in aqueous solutions of the nonionic surfactant “C₁₂E₆”—which includes hexagonal, cubic, lamellar, and micellar mesophases—has been studied by pulsed-field-gradient NMR. Diffusion coefficients were measured in unaligned samples in all of these phases. They were also obtained in the hexagonal and lamellar phases in oriented monodomain samples that were aligned by slow cooling from the micellar phase in an 11.7 T magnet. Measured water and soap diffusion coefficients in the NMR-isotropic cubic and (high-water-content) micellar phases as well as diffusion anisotropy measurements in the magnetically aligned hexagonal phase were quantitatively consistent with the constituent structures of these phases being identical surfactant cylinders, with only the fraction of surface-associated water varying with the water–soap molar ratio. The values of the water and soap diffusion coefficients in the oriented lamellar phase suggest an increase in defects and obstructions to soap diffusion as a function of increasing water content, while those in the low-water-content micellar phase rule out the presence of inverse micelles.

1. Introduction

Mesophases formed of amphiphilic surfactant molecules present a rich array of ordered structures composed of liquids in restricted geometries. Ordered structures in amphiphilic systems are the building blocks of living matter, and the relation between structure and transport is both interesting and important. While structure^{1,2} and diffusion^{3–5} in these systems have been studied extensively, “sample-memory” effects relating to slow domain-coarsening dynamics complicate the quantitative measurements. Only a few studies have explicitly looked at the anisotropic dynamics in oriented single domains,^{6–8} and this primarily in lamellar and membrane phases (see ref 9 for a review). Measurements of anisotropic diffusion in samples with controlled macroscopic domain orientation would thus be useful in examining the consistency of the structures proposed for different phases.

Aqueous solutions of nonionic surfactant allow one to study purely entropic geometric effects without electro-

static effects playing a role. The C₁₂E₆/water system (Figure 1: temperature/W₀ phase diagram, where W₀ is the water–surfactant molar ratio, presented before by several groups^{4,5,10–14}) is attractive for this reason and also because it presents numerous mesophases as one varies surfactant concentration and temperature. Other nonionic surfactant systems with similar phases and phase transitions have also been recently studied.^{3,15,16} Such systems have great medical potential; for example, surfactant cubic phases are being studied as a biocompatible matrix for the slow release of drugs by various routes.¹⁷

Translational diffusion is the most fundamental form of transport in condensed matter, and pulsed-field-gradient nuclear magnetic resonance is a powerful, noninvasive probe of an ensemble-averaged diffusion coefficient (see refs 18 and 19 for recent reviews). In a previous work, field-cycling relaxation measurements²⁰ in the C₁₂E₆/D₂O system provided limits on structure in different mesophases, albeit in the context of a parameter-rich model. In this work, we obtain information on dynamics, in both the water and surfactant components,

* Corresponding author. Present address: Department of Physics and Physical Oceanography, Memorial University of Newfoundland, St. John's, NF, A1B 3X7, Canada.

[†] University of British Columbia.

[‡] CNR Research Area of Rome.

(1) Toledano, P.; Figueiredo Neto, A. M., Eds. *Phase Transitions in Complex Fluids*; World Scientific: River Edge, NJ, 1998.

(2) Raçon, Y.; Charvolin, J. *J. Phys. Chem.* **1988**, *92*, 6339.

(3) Geil, B.; Feiweier, T.; Pospiech, E.-M.; Eisenblatter, J.; Fujara, F.; Winter, R. *Chem. Phys. Lipids* **2000**, *106*, 115.

(4) Constantin, D.; Oswald, P.; Imperor-Clerc, M.; Davidson, P.; Sotta, P. *J. Phys. Chem. B* **2001**, *105*, 668.

(5) Gaemers, S.; Bax, A. *J. Am. Chem. Soc.* **2001**, *123*, 12343.

(6) Lindblom, G.; Wennerstrom, H. *Biophys. Chem.* **1977**, *6*, 167.

(7) Roeder, S. B. W.; Burnell, E. E.; Kuo, A.-L.; Wade, C. G. *J. Chem. Phys.* **1976**, *64*, 1848.

(8) Wasterby, P.; Oradd, G.; Lindblom, G. *J. Magn. Reson.* **2002**, *157*, 156.

(9) Oradd, G.; Lindblom, G. In *NMR of Ordered Liquids*; Burnell, E. E., de Lange, C. A., Eds.; Kluwer Academic: Dordrecht, The Netherlands, 2003.

(10) Tiddy, G. J. T. *Phys. Rep.-Rev. Sect. Phys. Lett.* **1980**, *57*, 2.

(11) Mitchell, D. J.; Tiddy, G. J. T.; Waring, L.; Bostock, T.; McDonald, M. P. *J. Chem. Soc., Faraday Trans. 1* **1983**, *79*, 975.

(12) Fairhurst, C. E.; Holmes, M. C.; Leaver, M. S. *Langmuir* **1997**, *13*, 4964.

(13) Capitani, D.; Casieri, C.; Briganti, G.; la Mesa, C.; Segre, A. L. *J. Phys. Chem. B* **1999**, *103*, 6088.

(14) Briganti, G.; Capitani, D.; Segre, A. L.; Casieri, C.; La Mesa, C. *J. Phys. Chem. B* **1999**, *103*, 825.

(15) Hamley, I. W.; Castelletto, V.; Mykhaylyk, O. O.; Yang, Z.; May, R. P.; Lyakhova, K. S.; Agur Sevinc, G. J.; Zvelindovsky, A. V. *Langmuir* **2004**, *20*, 10785.

(16) Feiweier, T.; Geil, B.; Pospiech, E.-M.; Fujara, F.; Winter, R. *Phys. Rev. E* **2000**, *62*, 8182.

(17) Shah, J. C.; Sadhale, Y.; Chilukuri, D. M. *Adv. Drug Delivery Rev.* **2001**, *47*, 229.

(18) Price, W. S. *Concepts Magn. Reson.* **1997**, *9*, 299.

(19) Price, W. S. *Concepts Magn. Reson.* **1998**, *10*, 197.

(20) Burnell, E. E.; Capitani, D.; Casieri, C.; Segre, A. L. *J. Phys. Chem. B* **2000**, *104*, 8782.

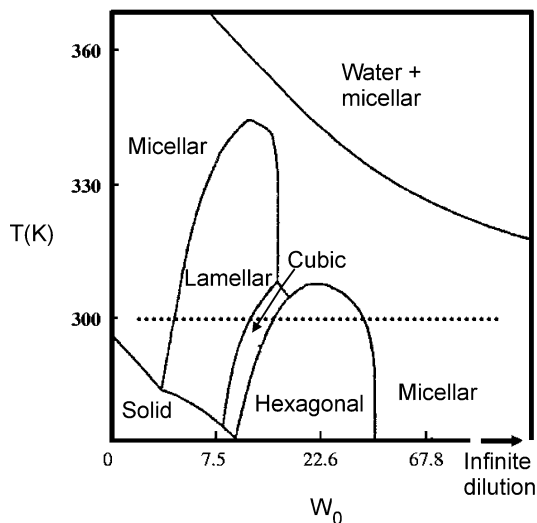


Figure 1. Phase diagram of aqueous solutions of $C_{12}E_6$, $CH_3-(CH_2)_{11}-(OCH_2CH_2)_6-OH$, as a function of $H_2O-C_{12}E_6$ molar ratios, W_0 , and temperature. At 300 K (dotted line), the phase sequence upon decreasing W_0 is micellar-hexagonal-cubic-lamellar-micellar.

from translational diffusion measurements in unaligned samples as well as diffusion and diffusion anisotropy in macroscopically aligned samples using pulsed-field-gradient NMR.

2. Experimental Section

2.1. Sample Preparation and Calibrations. $C_{12}E_6/H_2O$ and $C_{12}E_6/D_2O$ samples were prepared with $C_{12}E_6$, $CH_3(CH_2)_{11}-(OCH_2CH_2)_6OH$ (Tokyo Kasei, Japan, used as received), fresh distilled H_2O , and D_2O (99.9%, used as purchased) at several compositions with different water to surfactant molar ratios, W_0 . The $C_{12}E_6$ /water mixture was first prepared in glass vials which were weighed on a mechanical balance (least significant digit 0.01 mg) initially and after the addition of each component, temporarily sealed with wax film ("Parafilm"), and mixed with Teflon-coated stir bars on a hot plate/magnetic stirrer. The sample was then pipetted warm (using warm pipets as well) into a homemade round-bottom glass tube. After filling, the top was carefully flame-sealed while the bottom of the tube with the sample was water-cooled to prevent evaporation. Once sealed and cooled, the sample was warmed to ≈ 315 K (an isotropic micellar phase for $W_0 > 15$ and $W_0 < 5$, see Figure 1) and centrifuged a few times in opposite directions for further homogenization. This was the inner cylinder in a concentric cylinder geometry. The inner cylinder fit snugly into the outer cylinder (a standard NMR tube), with enough space in between for a liquid (10% $CHCl_3$ in $CDCl_3$) which was usable as a diffusion reference.

We used 99.9% D_2O ($D_0^{HDO-D_2O} = 1.902 \times 10^{-9} \text{ m}^2/\text{s}$) at 298 K for absolute calibration of the gradient.^{19,21} In samples with the concentric glass-tube geometry, 10% $CHCl_3$ in $CDCl_3$ was in some cases used as a gradient reference. These references were cross-calibrated (Table 1) against trace HDO in D_2O . A gradient calibration using a sample of 99.9% D_2O /10% $CHCl_3$ in $CDCl_3$ in concentric inner/outer tubes at 300 K was carried out in conjunction with each experimental run.

The experiments were performed on Bruker AMX500 and AV400 spectrometers (with proton Larmor frequencies at 500.13 and 400.13 MHz) with results that were checked to be mutually consistent. Convection effects (reported in similar studies)²² were not found to affect the results in either the viscous $C_{12}E_6$ /water samples or the calibration standards. The temperature on both spectrometers is controlled by a commercial air-flow system. Apart from the variable temperature experiments and the

Table 1. Diffusion Cross-Calibration Values, D^{a-b} / $D_0^{HDO-D_2O}$, Measured in This Work Where D_0^{a-b} Refers to the Diffusion Coefficient of a in Bulk Liquid b (Trace Amounts in the Case of $D_0^{HDO-D_2O}$)^a

T	$a-b$			
	HDO-D ₂ O	H ₂ O-H ₂ O	D ₂ O-D ₂ O	10% CHCl ₃ -CDCl ₃
298 K	1.0	1.209(5)	0.984(2)	
300 K	1.059(5)	1.264(7)	1.042(2)	1.281(20)

^a All values are relative to $D_0^{HDO-D_2O} \equiv 1.902 \times 10^{-9} \text{ m}^2 \text{ s}^{-1}$ at 298 K²¹ for trace HDO in pure D_2O .

experiments in section 3.4, the temperature was maintained at 300 K. We used a temperature calibration standard before each experiment and defined 300 K to be the temperature at which the splitting in a dimethyl sulfoxide (DMSO)/ethylene glycol temperature standard was 1.4922 ± 0.0006 ppm (746.3 ± 0.3 Hz on the AMX500 spectrometer and 597.1 ± 0.3 Hz on the AV400 spectrometer). The corresponding temperature repeatability is ± 0.05 K.

2.2. NMR Experiments. In all samples, we obtain diffusion coefficients for the water and the surfactant components simultaneously. We use a pulsed-field-gradient stimulated echo pulse program²³ to measure diffusion: $(\pi/2)_x - \tau_1 - (\pi/2)_x - \tau_2 - (\pi/2)_x - \tau_1 - \text{echo}$. Sinusoidal pulsed gradients of duration δ and peak amplitude g are applied during the τ_1 durations $5 \mu\text{s}$ after the first and third $\pi/2$ pulses. The peaks of the sinusoidal gradient pulses are separated by the time $\Delta = \tau_1 + \tau_2$. A square homogeneity-spoiling gradient of duration δ_{spoil} , applied during the τ_2 durations $5 \mu\text{s}$ after the second $\pi/2$ pulse, removes unwanted transverse coherences during the "z-storage" time. The gradient steps were varied in 32 steps to a maximum gradient amplitude of ≈ 50 G/cm and in 16 steps to 15% of the maximum gradient in successive experiments in one experimental run. Some of the results in section 3.1 were obtained using a spin-echo pulse sequence with mutually consistent results.

Experiments were typically carried out for three values of diffusion time, $\Delta' \equiv \Delta - \delta/4$ (ranging from 50 to 400 ms). Gradient pulse durations, δ , of 10, 6, or 3 ms were tried with consistent results; $\delta = 6$ ms was most frequently used. The spectra were obtained with a spectral window of 15 kHz, and the free-induction decay (FID) was multiplied by an exponential line broadening factor equivalent to 1 Hz prior to Fourier transformation. The signal strength, S , at each gradient amplitude was obtained by peak integration. The diffusion coefficient is obtained from the following equation for the attenuation of the signal:

$$\ln(S/S_0) = -(4/\pi^2)\gamma^2 g^2 D \delta^2 (\Delta - \delta/4) \quad (1)$$

where the gradient pulse is sinusoidal in shape and $g = mg_{\text{max}}$ is the gradient pulse amplitude, with m being a fraction between 0.01 and 1 in minimal steps of 0.01. γ is the magnetogyric ratio ($\gamma_{1H} = 26.752 \times 10^7 \text{ s}^{-1} \text{ T}^{-1}$ and $\gamma_{2H} = 4.107 \times 10^7 \text{ s}^{-1} \text{ T}^{-1}$).

3. Results

We obtain diffusion coefficients for the water and the alkyl ($CH_3(CH_2)_{11}$) and oxyethylene ($OCH_2CH_2)_6$) parts of the surfactant. The alkyl and oxyethylene peaks are found, unsurprisingly, to have identical diffusion coefficients, so we simply integrate both peaks at once. In the NMR-isotropic phases, the water and surfactant components are spectrally separated and these integrations are trivial. In the anisotropic phases, there is overlap between the water and surfactant signals. The results thus have to be fit to biexponentials. This poses no difficulties because the water and surfactant diffusion coefficients are not close in magnitude. We first obtain diffusion coefficients for each chemical species in macroscopically unaligned samples (Figure 2). All values are relative to $D_0^w \equiv D_0^{H_2O-H_2O}$ at 300 K.

(21) Holz, M.; Weingartner, H. *J. Magn. Reson.* **1991**, *92*, 115.

(22) Esturau, N.; Sanchez-Ferrando, F.; Gavin, J. A.; Roumestand, C.; Delsuc, M.-A.; Parella, T. *J. Magn. Reson.* **2001**, *153*, 48.

(23) Tanner, J. E. *J. Chem. Phys.* **1970**, *52*, 2523.

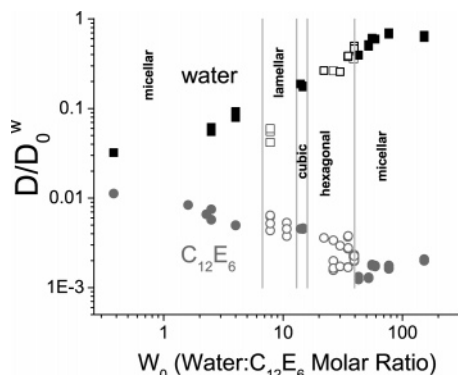


Figure 2. Diffusion coefficient vs W_0 in the $C_{12}E_6/H_2O$ phase diagram for unaligned samples at 300 K. Squares/circles are diffusion coefficients of the water/ $C_{12}E_6$ components. Solid symbols indicate that the soap spectrum in that sample displayed narrow peaks characteristic of spins undergoing isotropic tumbling.

3.1. Diffusion vs W_0 : Macroscopically Unaligned Samples at 300 K. Figure 2 shows the diffusion coefficients of both the water (squares) and soap (circles) components as a function of the water– $C_{12}E_6$ molar ratio, W_0 . In powder samples, one would normally not expect the echo amplitude to exhibit a simple monoexponential decay from which to extract a single isotropic diffusion coefficient. The observation of a pure monoexponential decay in our experiments indicates that the domain sizes are smaller than a “diffusion length scale”

$$l = \sqrt{2D\Delta'} \quad (2)$$

calculated from the slowest measured diffusion coefficient of the particular sample and the duration $\Delta' = \Delta - \delta/4 \approx 50$ ms of the shortest stimulated echo experiment. Samples which displayed a *soap* spectrum with narrow peaks characteristic of spins undergoing isotropic tumbling are denoted with filled symbols, while the others have open symbols.

The *surfactant* diffusion is at its highest in its pure state ($W_0 \approx 0$), representing the molecular diffusion of surfactant in three dimensions. As the water concentration increases, the volume available for the surfactant is reduced, and thus, the trend is for the surfactant diffusion to slow with increasing water content. The *water* diffusion is highest at large W_0 , approaching the molecular diffusion of water in three dimensions. We track the diffusion coefficients as we span the phase diagram of Figure 1 at 300 K:

(1) **Micellar phase:** $W_0 > 39$. The micellar phase is “NMR-isotropic”; that is, it exhibits a high-resolution NMR spectrum with the water peak well separated from the alkyl and oxyethylene peaks. Due to rapid exchange, this water peak includes signals from the water as well as the OH group of the $C_{12}E_6$. The relative peak intensities in a one-dimensional spectrum give a measure of W_0 that is in agreement (to within 5%) with that determined by weighing. Water diffusion increases from $D^w/D_0^w \approx 0.4$ close to the hexagonal–micellar phase transition toward unity at large W_0 . The soap diffusion in the micellar phase also increases with increasing W_0 , with the soap-to-water diffusion ratio *remaining constant* (Figure 3).

(2) **Hexagonal phase:** A monoexponential decay and a single isotropic diffusion coefficient are observed. Over the shortest time scale $\Delta' = 50$ ms of our measurement and at the measured soap diffusion coefficient $D^s = 7 \times 10^{-12}$ m²/s, the corresponding diffusion length scale $l \approx 0.8$ μ m is an upper limit for the domain size. Water

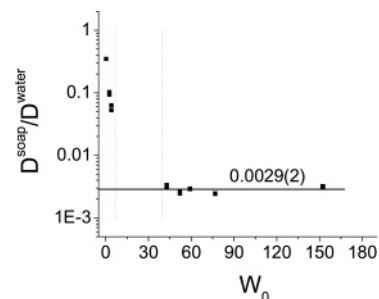


Figure 3. Diffusion in the micellar phase at 300 K. The ratio of soap-to-water diffusion is plotted vs W_0 in the two micellar phases. In the low- W_0 phase, this ratio decreases with increasing W_0 , while, in the high- W_0 micellar phase, this ratio appears to be constant.

diffusion in the hexagonal phase continues to decrease with decreasing W_0 . Soap diffusion exhibits a large statistical variation in measured diffusion coefficient values.

(3) **Cubic phase:** The cubic phase has an isotropic NMR spectrum. The reduced diffusion coefficients (shown in Figure 2) have the values $D^w/D_0^w = 0.19$ and $D^s/D_0^w = 0.0046$. The continuity of the water diffusion coefficients, as a function of W_0 , with those in the hexagonal phase suggests that the water remains a continuous subphase. The large soap diffusion coefficient suggests that the surfactant is also a continuous subphase, consistent with the accepted notion that the cubic phase is “bicontinuous”.²⁴

(4) **Lamellar phase:** Surfactant diffusion in the lamellar phase is higher, but of the same order of magnitude, than that in the cubic phase. Water diffusion, however, is significantly (a factor of ≈ 2) lower than that in the cubic phase.

(5) **Micellar phase:** $W_0 < 7$. Surfactant diffusion continues to increase with decreasing W_0 , approaching the pure surfactant diffusion value. Since we do not dry the surfactant, the lowest value of W_0 we achieve is $W_0 = 0.39$. This yields the reduced diffusion coefficients $D^w/D_0^w = 0.032$ and $D^s/D_0^w = 0.011$. The soap-to-water diffusion ratio is *not constant* (Figure 3). The water diffusion coefficient increases with increasing W_0 . This W_0 dependence is contiguous with the trend at higher W_0 in the cubic, hexagonal, and micellar phases. However, there is a break across the micellar–lamellar transition: water diffusion in this micellar phase is significantly faster than that in the lamellar phase.

There is significant statistical variation in the values of surfactant diffusion coefficients in the lamellar and hexagonal phases. This was initially conjectured to be due to partial ordering; that is, they are not true “powder” samples. To simplify the picture, we prepared samples with D_2O instead of H_2O and then studied macroscopically aligned samples prepared (as in refs 13 and 14) by slow cooling from a high-temperature micellar phase in the presence of an external magnetic field.

3.2. Creation and Characterization of Magnetically Aligned Monodomain Samples. The $C_{12}E_6/H_2O$ (or D_2O) phase diagram at 300 K has three NMR-isotropic phases (a cubic and two micellar phases) and two phases (the hexagonal and lamellar phases) with broad $C_{12}E_6$ spectra. The creation of a fully aligned lamellar phase¹⁴ and a partially oriented hexagonal phase¹³ has been previously reported upon cooling from the isotropic phase. In this work, we were able to *completely* magnetically

(24) Lindblom, G.; Rilfors, L. *Biochim. Biophys. Acta* **1989**, *988*, 221.

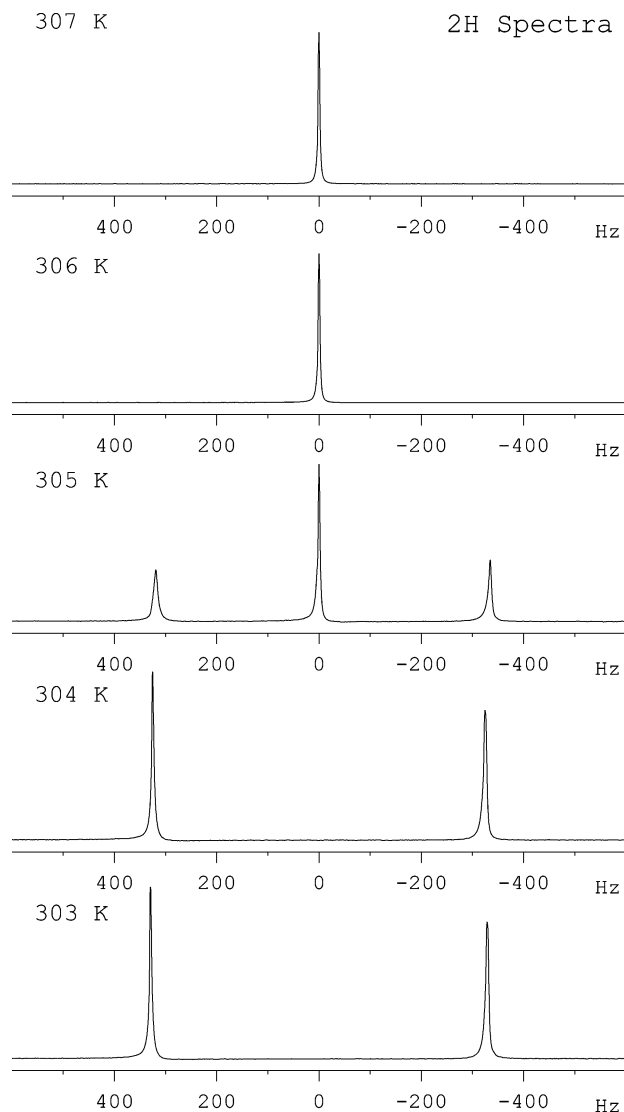


Figure 4. Deuteron (^2H) NMR spectrum at temperatures spanning the micellar–hexagonal transition. ($\gamma_{2\text{H}}/2\pi$) $B_0 = 76.77$ MHz. $\text{C}_{12}\text{E}_6/\text{D}_2\text{O}$, $W_0 = 35$. The top two spectra show a micellar phase, and the bottom two, a parallel-oriented hexagonal phase. The single doublet is evidence of single-domain orientation. Two-phase coexistence is seen in the third spectrum from the top.

align both the lamellar phase *and* the hexagonal phase. Deuterium NMR was used on samples prepared with D_2O as a sensitive way to characterize this orientational order (see Figure 4).

In an oriented phase composed of bilayers, the surfactant has an anisotropic influence on the water molecules, so the water O–D bonds do not have zero average order parameter, that is, $S_{\text{OD}} \equiv \langle P_2(\cos(\alpha)) \rangle \neq 0$, where α is the angle made by a water OD bond with respect to the bilayer surface normal.

The splitting due to the quadrupolar interaction is approximated as

$$\Delta\nu_Q(\theta) = \frac{3}{2}(e^2qQ/h)S_{\text{OD}}P_2(\cos(\theta)) \quad (3)$$

where θ is the angle between the layer normal and the magnetic-field direction. For the sake of simplifying the discussion here, we ignore the asymmetry of the deuterium quadrupole tensor in D_2O .²⁵ We use a quadrupole coupling constant for the O–D bond of $e^2qQ/h \approx 220$ kHz.²⁶ S_{OD}

varies with the surfactant–water molar ratio, W_0 , and is not known, while $P_2(\cos(\theta))$ varies from 1 when the layer normal is parallel to the field direction ($\theta = 0$) to $-1/2$ when the layer normal is perpendicular ($\theta = \pi/2$). Note that the deuteron on the water molecule is exchanging with the surfactant headgroup on a time scale of a few milliseconds³ and only a single average peak is observed.

In the hexagonal and lamellar phases, the observed spectrum contains sets of doublets

$$\nu(\theta) = \nu_{\text{Zeeman}} \pm \Delta\nu_Q(\theta)/2 \quad (4)$$

for each orientation angle, θ . For an NMR-isotropic phase, an individual spin samples many orientations over the duration of experimental observation and sees an average, $\langle P_2(\cos(\theta)) \rangle = 0$, giving only a single peak at ν_{Zeeman} . A single-domain mesophase contains a single doublet, while a powder pattern exhibits the so-called Pake pattern.

In a hexagonal phase composed of cylinders, the surface normal does not coincide with the cylinder axis, and rapid diffusion about this axis introduces the additional term $\langle P_2(\cos(\beta)) \rangle$, where $\beta = \pi/2$ is the angle between the surface normal and the cylinder axis, giving an additional factor of $-1/2$ to the right-hand side of eq 3.

The top two spectra in Figure 4 show the single-peak isotropic spectrum in the micellar phase, while the bottom two spectra show the doublet of the aligned hexagonal phase. From the observed splitting with $\theta = 0$, we obtain $S_{\text{OD}} \approx 0.004$ at $W_0 = 35$.

In the oriented lamellar phase (at $W_0 = 6.7$), we obtain a doublet due to the quadrupolar splitting. Here, the surface normal (which is also the symmetry axis in the lamellar phase) is oriented at an angle of $\theta = \pi/2$. From the observed splitting (spectrum not shown) and using eq 3, we calculate an order parameter of $S_{\text{OD}} = 0.008$.

3.3. Diffusion Anisotropy in the Hexagonal Phase.

We prepared a sample in the hexagonal phase where we could measure diffusion parallel and perpendicular to the orientation direction. To achieve this in a single-axis gradient probe, our sample preparation method was as follows. Sample material prepared at a concentration corresponding to $W_0 = 30$ was filled (halfway) into a 2.5 cm long (one-side-sealed) glass tube. The other side was then carefully flame-sealed with water cooling applied to the bottom half of the tube. The sealed tube resembled a “bullet” which slid down almost snugly into a standard high-resolution NMR tube. The ^1H NMR spectrum was broader than usual even in the micellar phase. This is because of the magnetic-field inhomogeneity arising from the rounded edges of the bullet sample. Diffusion was measured in the proton channel, while the quality of monodomain orientation was monitored via the deuteron spectrum. In this aligned sample, we were unable to completely separate the water and soap signals in the proton spectrum. We divide the integration into two regions (with no gaps in between), a water-rich region and a soap-rich region. While there is not much signal outside these regions, there is significant overlap between these two regions. We thus fit the signal attenuation curves to biexponentials. Using diffusion times of $\Delta' = 50, 250,$ and 400 ms, we are able to clearly separate out the water diffusion from the soap diffusion. The sample was pretreated in three distinct ways:

(1) “Powder”: The sample was heated into the micellar phase and cooled slowly into the hexagonal phase *outside* the magnet.

(25) Abdolall, K.; Burnell, E. E.; Valic, M. I. *Chem. Phys. Lipids* **1977**, *20*, 115.

(26) Seelig, J. Q. *Rev. Biophys.* **1977**, *10*, 353.

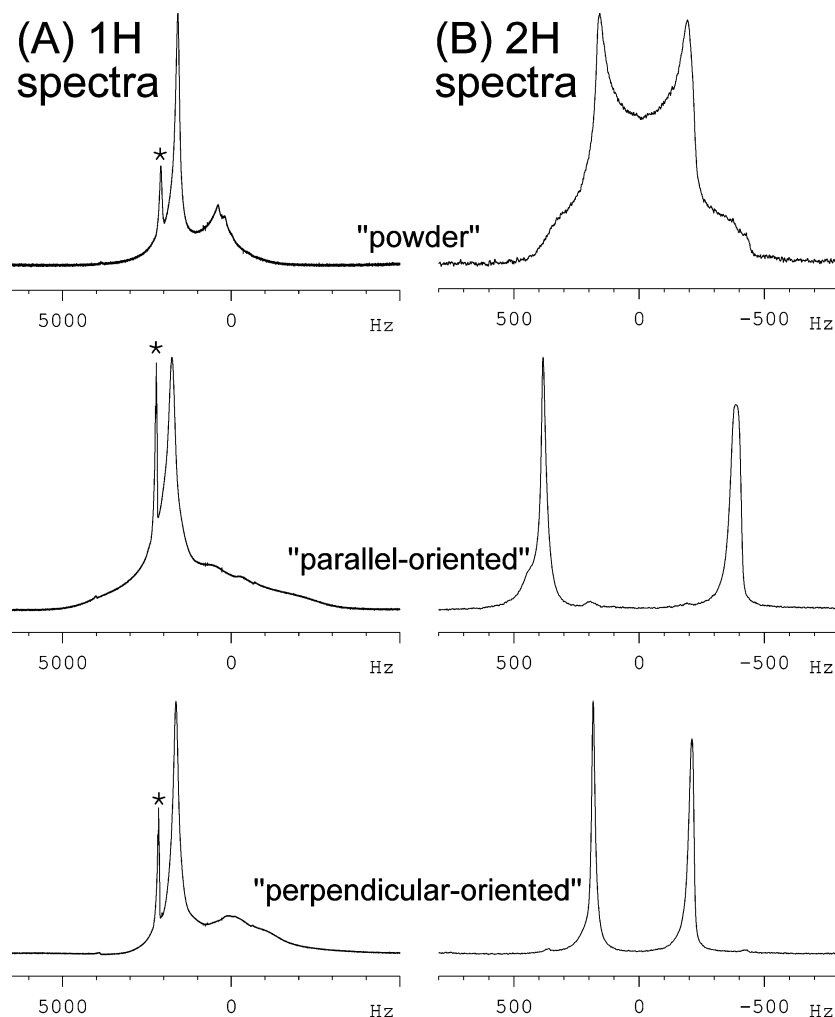


Figure 5. Going from top to bottom, one-dimensional spectra of powder, parallel-oriented (the monodomain orientation angle with respect to the magnetic field, $\theta = 0^\circ$), and perpendicular-oriented ($\theta = 90^\circ$) samples of $W_0 = 30$ (hexagonal phase): (A) Proton spectrum shows broad peaks corresponding to the soap (with the powder, top, displaying the super-Lorentzian²⁷ line shape) as well as a sharp peak corresponding to HDO (marked with an asterisk). $(\gamma_{1H}/2\pi)B_0 = 500.13$ MHz. (B) Deuteron spectrum (D_2O signal) shows the quadrupolar splitting pattern corresponding to powder, parallel-oriented, and perpendicular-oriented samples. The ratio of splittings at $\theta = 0$ and 90° is 2:1, as expected. $(\gamma_{2H}/2\pi)B_0 = 76.77$ MHz.

(2) “Parallel oriented”: The sample was heated into the micellar phase and slowly cooled into the hexagonal phase inside the 11.7 T magnet.

(3) “Perpendicular oriented”: The sample was placed in a radial hole cut into a cylindrical delrin rod and heated into the micellar phase, and the rod was quickly lowered into the 11.7 T magnet while the temperature was maintained above the micellar transition temperature. The sample was then cooled into the hexagonal phase with the bullet axis oriented perpendicular to the magnetic field. The rod was then removed and the sample placed inside a standard NMR tube. Now, the orientation was perpendicular to the NMR tube (and thus the magnetic field) axis.

Proton and deuteron spectra obtained after the three pretreatments are shown in Figure 5. The proton spectrum (Figure 5A, top) of the powder shows the characteristic “super-Lorentzian”²⁷ line shape, while the deuteron spectrum (Figure 5B, top) shows the Pake doublet. The deuteron spectrum in the parallel- and perpendicular-oriented samples shows simple doublets with splittings of $\Delta\nu_{\parallel} = 768.4$ Hz and $\Delta\nu_{\perp} = 394.3$ Hz. The ratio $\Delta\nu_{\parallel}/\Delta\nu_{\perp}$

$= 1.95$ is close to that expected, namely, $|(3 \cos^2(0^\circ) - 1)/(3 \cos^2(90^\circ) - 1)| = 2$.

3.3.1. Water Diffusion. The diffusion coefficient of the water peak in the hexagonal phase was measured in a bullet sample at $W_0 = 30$ that was sequentially an unaligned powder and then magnetically aligned with the cylinder axis parallel and perpendicular to the magnetic field. For the experimentally measured diffusion coefficients, the superscript “w”, used for the aqueous component, is dropped in what follows in this section while every “s” superscript, for the $C_{12}E_6$ component, is retained. The superscript “c” denotes calculated values. The parallel-oriented sample exhibited a higher water diffusion than the perpendicular-oriented sample. This is consistent with a picture of water diffusing in the presence of obstructions. We define

$$D_{ii}^c/D_0^w = A_{ii}(1 - f) \quad (5)$$

where A_{ii} are the obstruction factors ($A_{xx} = A_{yy} \equiv A_{\perp}$ and $A_{zz} \equiv A_{\parallel}$), D_0^w is the diffusion coefficient of bulk water, and f is the fraction of water that is assumed to be “surface-associated”.²⁸ This is similar but not identical to ref 29. The factor $1 - f$ arises from the assumption that the

(27) Bloom, M.; Burnell, E. E.; Roeder, S. B. W.; Valic, M. I. *J. Chem. Phys.* **1977**, *66*, 3012.

surface-associated water exchanges with the free water rapidly on the time scale of the NMR measurement.

For cylindrical obstructions, both an effective cell approximation and a solution of the diffusion equation (with no long-range interaction terms included) employing a truncated Rayleigh multipole expansion (see ref 29) give identical results at volume fractions less than $\phi = 0.65$.

$$A_{\parallel} = 1$$

$$A_{\perp} = \frac{1}{1 - \phi'} \left(1 - \frac{2\phi'}{1 + \phi' - s(\phi')} \right) \quad (6)$$

In the simplest picture, $\phi' = \phi$, where ϕ is the surfactant volume fraction and is related to the molar ratio, W_0 , as

$$\phi = \frac{1}{1 + W_0(M^w/M^s)/(\rho^w/\rho^s)} = \frac{1}{1 + W_0/21.43} \quad (7)$$

where $M^w = 20.03$ and $M^s = 450.65$ are the D_2O and surfactant molecular weights and ρ^w and ρ^s are the water and $C_{12}E_6$ relative densities. The term $s(\phi)$ is zero in the mean-field approximation, while, for a hexagonal lattice of cylinders, $s(\phi) = 0.07542\phi^6$ up to order ϕ^6 . For $\phi = 0.4167$ (calculated using eq 7, $W_0 = 30$), $s(\phi) = 0.0003$, thus justifying the mean-field approximation in comparison to experiment.

This gives anisotropic diffusion coefficients.

$$D_{\parallel}^c/D_0^w = 1 - f$$

$$D_{\perp}^c/D_0^w = \frac{1 - f}{1 + \phi'} \quad (8)$$

Since a fraction, f , of the water is surface-associated, the true excluded volume, ϕ' , must account for this. We assume that water forms x monolayers of total thickness xd at a water–surfactant interface on the surface of a surfactant cylinder of radius r and length L , where $d = 0.3$ nm is the thickness of a water monolayer.

To estimate the radius, r , we use model estimates (refs 30 and 31) for the hydrocarbon radius of $r_{hc} = 1.3$ nm. We then assume a maximally packed oxyethylene hydrophilic part (it is known in fact that this “headgroup” gets hydrated and extended, but we account for that via the water layer x). Using the relative masses of the “hydrocarbon” and headgroup parts (169.33 and 281.32) and the relative maximal densities—here, we use the density of dodecane $\rho_{\text{dodecane}} = 0.7546$ and of poly(ethylene glycol) (PEG) $\rho_{\text{PEG}} \approx 1.15$ —we get the volume ratio

$$\frac{V_{hc} + V_{hg}}{V_{hc}} = \frac{\frac{169.33}{0.7546} + \frac{281.32}{1.15}}{\frac{169.33}{0.7546}}$$

$$= 2.09 \quad (9)$$

From this, we can calculate the bare (unhydrated) cylinder radius $r = r_{hg} + r_{hc}$ (where “hc” and “hg” refer to hydrocarbon and headgroup, respectively) using the relation

$$\frac{r_{hc} + r_{hg}}{r_{hc}} = \sqrt{\frac{V_{hc} + V_{hg}}{V_{hc}}}$$

$$= 1.4457 \quad (10)$$

Thus, the bare cylinder radius, r , is $1.4457r_{hc} = 1.88$ nm. The “hydrated” cylinder then has the radius $R = r + xd$, where x will be determined by the fraction of surface-associated water, f .

$$f = \frac{\phi\pi L[(r + xd)^2 - r^2]/\pi r^2 L}{1 - \phi}$$

$$= \left(\frac{2xd}{r} + \frac{x^2 d^2 21.43}{r^2 W_0} \right) \quad (11)$$

The volume excluded to (the center of mass of) a water molecule is then a cylinder of radius $r + xd + d/2 = r[1 + (d/r)(x + 0.5)]$. Therefore,

$$\phi' = \phi \left[1 + \frac{d}{r}(x + 0.5) \right]^2 \quad (12)$$

We also allow for cylinder undulations as follows. Provided the undulations are small, the local diffusion coefficients are given by eq 8, but the local “director” does not coincide with the magnetic-field direction (i.e., the direction of the diffusion measurement. We account for that by modifying the equations

$$D_{\parallel}^{c\beta}/D_0^w = (1 - f)(1 - \beta)$$

$$D_{\perp}^{c\beta}/D_0^w = \frac{1 - f}{1 + \phi'} + \frac{\beta}{2(1 - f)} \quad (13)$$

where the above equations satisfy $D_{\parallel}^{c\beta} + 2D_{\perp}^{c\beta} = D_{\parallel}^c + 2D_{\perp}^c$. β is now a fit parameter. We will replace the left-hand side in the two equations in eq 13 using the experimental values $D_{\parallel}/D_0^w = 0.414(5)$ and $D_{\text{isotropic}}/D_0 = (D_{\parallel}/D_0 + 2D_{\perp}/D_0)/3 = 0.346(5)$ (Table 2). We further replace f with eq 11 and ϕ' with eq 12 and calculate the parameters β and x . The above is evaluated for $d = 0.3$ nm, $r = 1.88$ nm, and $W_0 = 30$ (i.e., $\phi = 0.4167$). Solving numerically, we obtain

$$\beta = 0.16 \pm 0.03$$

$$x = 1.93 \pm 0.02 \quad (14)$$

The above value of x gives the fraction of surface-associated water $f = 0.51 \pm 0.02$. Estimates for the radius of the hexagonal cylinder cross section have varied from 1.4 nm³² to 2.4 nm.³⁰ The radius of the bare cylinder is $r = 1.88$ nm, while the radius of the hydrated cylinder is $R = r + xd = 2.46$ nm. This model of a hydrocarbon core, oxyethylene headgroup “shell”, and water “outer shell” is clearly not the actual structure. However, it is a useful device to estimate the volumes of the headgroup and surface-associated water relative to the hydrocarbon core. Our estimate for the hydrated cylinder radius uses our results and the radius of the hydrocarbon core in the work of ref 30 and agrees rather well with the value for the hydrated radius given in that work.

Also interesting is the fact that at $W_0 = 30$ we calculate $f/W_0 = 15.3$. Thus, given the above cylinder structure, at $W_0 = 15.3 \pm 0.03$, all water would be surface-associated. The transition to the cubic phase at $W_0 \approx 15$ and to the lamellar phase for lower W_0 thus makes sense.

(28) Clark, M. E.; Burnell, E. E.; Chapman, N. R.; Hinke, J. A. M. *Biophys. J.* **1982**, *39*, 289.

(29) Johannesson, H.; Halle, B. *J. Chem. Phys.* **1996**, *104*, 6807.

(30) Carale, T. R.; Blankshtein, D. *J. Phys. Chem.* **1992**, *96*, 459.

(31) Puvvada, S.; Blankshtein, D. *J. Chem. Phys.* **1990**, *92*, 3710.

(32) Carvell, M.; Hall, D. G.; Lyle, I. G.; Tiddy, G. J. *Trans. Faraday Discuss.* **1986**, *81*, 223.

Table 2. Diffusion Coefficients (from Proton Spectra) in the Hexagonal Phase ($W_0 = 30$) at 300 K: Powder (Unoriented) and Parallel- and Perpendicular-Oriented Samples^a

sample	D^w/D_0^w	D^s/D_0^s
hexagonal powder	HDO component 0.253(5)	$C_{12}E_6$ component 0.0029(1)
parallel	0.414(5)	0.0034(1)
perpendicular	0.312(5)	0.0008(1)

^a For this sample, the soap reference value is $D_0^w = D_0^{D_2O-D_2O}$ and the HDO reference value is $D_0^s = D_0^{HDO-D_2O}$. For the HDO component, we use $D^{D_2O-D_2O}/D_0^{D_2O-D_2O} = D^{HDO-D_2O}/D_0^{HDO-D_2O}$. Errors in the last digit, shown in parentheses, reflect the calculated error from a single diffusion signal attenuation plot. The sample-to-sample statistical variation in *aligned samples* is $\approx 5\%$. Powder samples show a much larger systematic variation ($\approx 50\%$ near the hexagonal-micellar transition) that reflects the sample history and the degree of partial ordering.

As seen in Table 2, both parallel- and perpendicular-oriented samples have a water diffusion coefficient that is larger than that in the unaligned powder sample. This is puzzling. According to the simplest picture, the powder sample is simply a collection of domains of different orientations. In this picture, assuming rapid exchange among domains, the diffusion coefficient measured for the powder should simply be a statistical average over all orientations ($D_{\text{powder}} = D_{\text{isotropic}} = (D_{\parallel} + 2D_{\perp})/3$). The isotropic value calculated from the measured diffusion anisotropy is

$$D_{\text{isotropic}}^c = D_{\parallel}(1 + 2D_{\perp}/D_{\parallel})/3 \approx (0.83 \pm 0.02)D_{\parallel} \quad (15)$$

where we used (from Table 2, HDO component) the experimental ratio $D_{\parallel}/D_{\perp} = 1.33 \pm 0.03$. Even if the measurement of the powder picks out a preferential direction between 0 and 90° (such as the magic angle) rather than a true random sampling, one expects that $D_{\perp} < D_{\text{powder}} < D_{\parallel}$, contrary to what was observed in our measurements (Table 2): $D_{\text{powder}} < D_{\perp} < D_{\parallel}$. One possibility is that there are significant restrictions to diffusion at the domain boundaries in the powder sample, not present in the monodomain samples. We note, additionally, that the water diffusion coefficient in the powder sample relative to that in the parallel-oriented sample is $D_{\text{powder}}/D_{\parallel} = 0.62 \pm 0.02$, roughly three-fourths of the value of 0.83 calculated in eq 15.

3.3.2. Soap Diffusion. The soap diffusion in the hexagonal phase powder sample (Table 2) is slower than that in the parallel-oriented sample. However, diffusion in the perpendicular-oriented sample is significantly slower than that in the others. This is consistent with our picture of soap molecules being constrained in the cylinder volume. In the “parallel” samples, the soap can diffuse in quasi-one-dimensional channels along the field direction. In the “perpendicular” samples, the field direction is perpendicular to the cylinder axis, so any measured diffusion may be identified with the rather slow motion of the entire cylinder or of diffusion through interconnections that run perpendicular to the cylinders as implied from tracer diffusion measurements.⁴ However, while the value of D_{\perp}^s is consistent with the value obtained from tracer diffusion measurements in ref 4, our value of D_{\parallel}^s is roughly a factor of 5 smaller than the tracer value. The reason for this discrepancy is unclear. The virtue in the NMR measurement is that these magnetically oriented samples are exceptionally well oriented, and the diffusion measurement is made noninvasively.

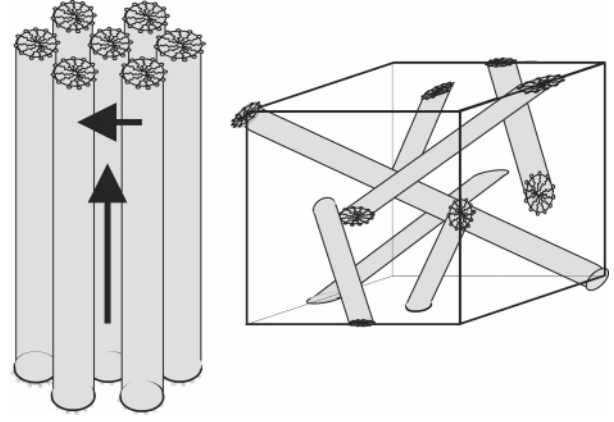


Figure 6. Cartoons illustrating the anisotropy of diffusion parallel and perpendicular to the long axis of perfect, oriented cylinders (left) and the model of close-packed cylinders in a body-centered cubic lattice (right) with the lattice spacing $a = 2\sqrt{2}(2r)$, where r is the cylinder radius. Such a construction is consistent with the $Ia3d$ space group.^{33,34} There are four sets of parallel cylinders shown. The angle between each set is the tetrahedral angle ($\approx 109.47^\circ$).

Table 3. Diffusion Coefficients (from Proton Spectra) at 298 K in (A) the Cubic Phase ($W_0 = 14.4$) and (B and C) the Perpendicular-Oriented Lamellar Phases ($W_0 = 12.2$ and $W_0 = 6.7$)^a

sample	D^w/D_0^w	D^s/D_0^s
(A) cubic	0.188(5)	0.0046(1)
(B) lamellar “ \perp ”, $W_0 = 12.2$	0.230(3)	0.0053(1)
(C) lamellar “ \perp ”, $W_0 = 6.7$	0.104(3)	0.0076(1)

^a Note that in the lamellar phase the layer normal aligns perpendicular to the magnetic field. Thus, D_{\perp} corresponds to diffusion along one of the two *easy* directions.

Once again, we can calculate an isotropic soap diffusion coefficient (as for water diffusion in eq 15):

$$D_{\text{isotropic}}^{\text{sc}} = \frac{D_{\parallel}^s + 2D_{\perp}^s}{3} \quad (16)$$

From Table 2, we obtain $D_{\text{isotropic}}^{\text{sc}}/D_0^w = 0.0017(1)$ (using eq 16). The actual value is $D_{\text{powder}}^s/D_0^w = 0.0029(1)$ (see Table 2), which is 1.7 ± 0.2 times larger.

3.4. Cubic and Oriented Lamellar Phases. It has been previously proposed that the building blocks of the cubic phase are consistent with the $C_{12}E_6$ being organized (see Figure 6) into cylinders close packed on a body-centered cubic lattice, with the angle between nonparallel cylinders being the tetrahedral angle ($\approx 109.47^\circ$). The structure shown is as described in refs 33 and 34 and belongs to the space group $Ia3d$, that is, the cubic-gyroid phase. Note that the cubic-gyroid phase is also consistent with the results of scattering experiments.³⁵ Using the above picture, one expects that the diffusion of a soap molecule is one-dimensional with only one-third of the time effectively spent along the z direction. If the surface-associated water layer were to play no role in soap diffusion, we would thus expect soap diffusion in the cubic phase to be $D^{\text{s,cubic}} \approx D_0^s/3$ (where D_0^s is the bulk $C_{12}E_6$ diffusion coefficient). Moreover, if the lamellar phase was composed of defect-free, unbounded sheets (with the layer normal perpendicular to the magnetic field), then the

(33) Andersson, S.; O’Keeffe, M. *Nature* **1977**, *267*, 605.

(34) O’Keeffe, M.; Plévert, J.; Ogawa, T. *Acta Crystallogr.* **2002**, *A58*, 125.

(35) Clerc, M.; Levelut, A. M.; Sadoc, J. F. *J. Phys. II* **1991**, *1*, 1263.

diffusion coefficient along the magnetic field in the *oriented sample* would equal the bulk surfactant diffusion coefficient measured, that is, $D_{\perp}^{s,\text{lamellar}} \approx D_0^s$.

From our measurement (Table 3A) $D_{\perp}^{s,\text{cubic}}/D_0^w = 0.0046$, we would expect the bulk surfactant diffusion coefficient to be $D_0^s/D_0^w = 0.0138$. The measured diffusion coefficient in neat $C_{12}E_6$ (from a spectrum integration, we determined $W_0 = 0.39$) was $D^s/D_0^w = 0.011 = 0.8D_0^s/D_0^w$, so this is consistent with the simple picture of the cubic phase described above.

We also measured diffusion in magnetically aligned samples in the lamellar phase at 298 K for concentrations corresponding to $W_0 = 12.2$ and $W_0 = 6.7$ (Table 3B,C). In a magnetic field, the lamellar phase orients with the layer normal perpendicular to the magnetic field: we thus denote this perpendicular alignment. The soap diffusion coefficients at the two concentration extremes of the oriented lamellar phase are $D_{\perp}^{s,\text{lamellar}}/D_0^w = 0.0053$ and $D_{\perp}^{s,\text{lamellar}}/D_0^w = 0.0076$. Thus, this value in the oriented lamellar phase is *always* significantly smaller than the bulk surfactant diffusion coefficient, which (using the value inferred from the measurement of $D^{s,\text{cubic}}$ at 298 K) is $D_0^s/D_0^w = 0.0132$.

The relatively low value of soap diffusion coefficient in the oriented lamellar phase suggests that the lamellar phase has defects in the soap structure (as suggested elsewhere^{2,20,36}) that serve as obstructions to soap diffusion. Such obstruction effects are not apparent in the cubic phase. It has been suggested that defects should be annealed out and that the soap diffusion coefficient should increase sharply close to the micellar transition.³⁶ Indeed, the oriented lamellar phase in the $W_0 = 6.7$ sample which is close to the lamellar–micellar coexistence region at 298 K has a soap diffusion coefficient that is 1.4 times larger than that of the $W_0 = 12.2$ oriented lamellar phase, but its value is still only 58% of D_0^s/D_0^w : there are thus still significant restrictions to diffusion.

The water diffusion coefficients add to this picture. In a perfectly aligned lamellar phase (with no surface-associated water), the water diffusion coefficient would have the bulk value, that is, unity. Instead, this value is $D^w/D_0^w = 0.1$ ($W_0 = 6.7$) and 0.23 ($W_0 = 12.2$). This implies (in this simplistic picture) that the fraction of surface-associated water, f , varies from 0.77 to 0.9 across the lamellar phase. Using an area per surfactant polar head of 0.52 nm^2 ³⁷ and surface area of a water molecule of 0.07 nm^2 corresponding to a water molecule radius of 0.3 nm, the number of surface-associated monolayers (assuming smooth lamellae) is

$$x = \frac{fW_0}{0.52/0.07} \quad (17)$$

Using eq 17, we obtain $x \approx 1.2$ ($W_0 = 12.2$) and $x \approx 0.8$ ($W_0 = 6.7$). At lower W_0 , almost all the water is surface-associated. A structural change leads to the formation of the micellar phase at lower W_0 . We conjecture that this change is driven by the fusing of lamellae due to incomplete water monolayers.

3.5. Temperature Dependence in Oriented Samples. We measured temperature dependencies across the micellar–hexagonal and micellar–lamellar transitions upon cooling. The low-temperature phases were prepared by slow cooling and were thus perfectly aligned. The

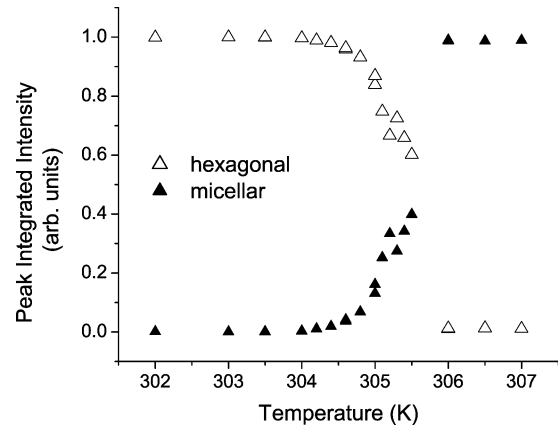


Figure 7. Integrated ^2H peak intensities for spectra as in Figure 4 for several temperatures spanning the micellar–hexagonal transition. $C_{12}E_6/D_2O$, $W_0 = 35$. Since the micellar and hexagonal phase signals are spectrally separated, the coexistence region can be studied quantitatively with deuterium NMR.

cylinder axis was parallel to the magnetic field in the hexagonal phase, while the surface normal was perpendicular to the magnetic field in the lamellar phase.

3.5.1. Hexagonal–Micellar Transition. At each temperature, we are able to separately integrate the spectrally separated hexagonal and/or micellar peaks. Indeed, in Figure 4, third from top, the deuterium NMR spectrum shows both the isotropic micellar peak and the doublet peaks of a monodomain hexagonal phase. We can thus follow the micellar–hexagonal phase transition (Figure 4), including the coexistence region, and we can plot the hexagonal and micellar peak intensities (Figure 7) as a function of temperature. The plot in Figure 7 shows a coexistence region of roughly 1–1.5 K (larger than any temperature variations across the sample volume inside the NMR probe which we estimate to be <0.5 K).

We now measure HDO (proton nucleus NMR) and D_2O (deuteron nucleus NMR) diffusion in the anisotropic environment of the magnetically aligned cylindrical surfactant obstructions. In the hexagonal phase as well as the micellar phase (lower and higher temperatures in Figure 8, part A for HDO and part C for D_2O), there is a roughly linear increase in the measured diffusion coefficient as a function of temperature. In fact, when we plot $\ln(D)$ versus $1/T$ (an Arrhenius plot, Figure 8B), we find that the dependence in both phases is consistent with a fixed slope of $2577 \pm 80 \text{ K}$. This value of the slope is not fitted; only the intercept (which is a multiplicative prefactor for the diffusion coefficient) is fit. The slope is held at the value for bulk water, obtained from a fit to the temperature dependence of *bulk* $D_{\text{HDO}-D_2O}$ (results not shown) in the temperature range of our measurements, and it corresponds to an activation energy

$$E_{\text{act}} = (2577 \pm 80)R \approx 21.4 \pm 0.6 \text{ kJ/mol} \quad (18)$$

where $R = 8.314 \text{ J K}^{-1} \text{ mol}^{-1}$ is the gas constant.

When the temperature dependence of the water diffusion coefficient in the micellar phase (at temperatures above the hexagonal phase of the $W_0 = 30$ sample at 300 K) is extrapolated to 300 K, we obtain the ratio $D_{\parallel}^{w,\text{micellar}}/D_{\parallel}^{w,\text{hexagonal}} \approx 0.8$ (Figure 8A). We also obtain the same ratio from measurements at the micellar–hexagonal coexistence point in Figure 8C. The *calculated* isotropic value from eq 15 is $D_{\text{isotropic}}^{wc} = 0.83D_{\parallel}^w$, and thus, $D_{\parallel}^{w,\text{micellar}} \approx D_{\text{isotropic}}^{wc}$. Thus, the micellar structure at high W_0 is quantitatively consistent with an orientationally isotropic

(36) Constantin, D.; Oswald, P. *Phys. Rev. Lett.* **2000**, *85*, 4297.

(37) Funari, S. S.; Holmes, M. C.; Tiddy, G. J. T. *J. Phys. Chem.* **1994**, *98*, 3015.

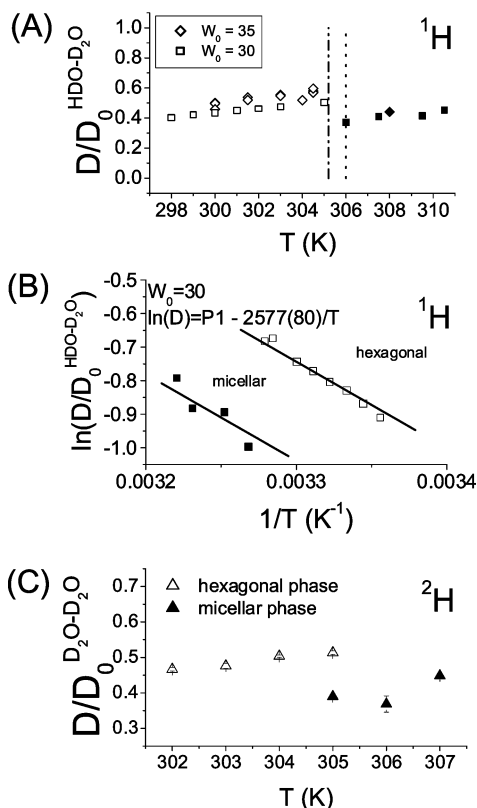


Figure 8. Diffusion in parallel-oriented samples ($W_0 = 30$ and 35) in the hexagonal phase: (A) Diffusion coefficient (proton, HDO component) vs T for $W_0 = 30$ and $W_0 = 35$, $C_{12}E_6/D_2O$. (B) The water diffusion is consistent with an Arrhenius linear $\ln(D)$ vs $1/T$ relationship (the values plotted are from the $W_0 = 30$ measurements in part A). The slope is not fitted: the bulk value for trace HDO in D_2O ($D_0^{HDO-D_2O}$) is used, with the intercept $P1$ being allowed to vary. (C) Diffusion coefficient (deuterium nucleus) vs T , $C_{12}E_6/D_2O$.

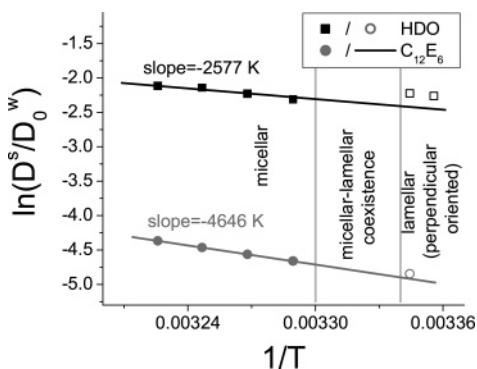


Figure 9. Diffusion in the micellar phase above the micellar–lamellar transition ($W_0 = 6.7$) also exhibits an Arrhenius temperature dependence that can be fit with a slope consistent with the activation energy of bulk water. The lamellar phase of this sample ($C_{12}E_6/D_2O$) run was oriented with the surface normal perpendicular to the magnetic field.

distribution of cylinders with the same surface-associated water fraction as that in the low-temperature hexagonal phase.

3.5.2. Micellar–Lamellar Transition. The temperature dependence of the water and soap diffusion coefficients in the micellar phase was investigated for a sample at a composition of $W_0 = 6.7$ (Figure 9) that exhibits a micellar–lamellar transition as a function of temperature. In the oriented lamellar phase, the doublet in the deuterium NMR spectrum corresponds to an orientation of the

lamellar structure such that the surface normal is perpendicular to the magnetic field. Water diffusion is measured along the magnetic-field direction, which in this geometry is one of the two “easy diffusion” directions perpendicular to the surface normal; in the absence of surface association, this value should equal unity. In the micellar phase, the isotropic diffusion coefficient is measured. The temperature dependence can once again be fit to an Arrhenius behavior with an activation energy of bulk water.

Since the structure of the high- W_0 micellar phase (the high-temperature phase above the hexagonal phase) is consistent with the orientationally isotropic version of the hexagonal phase, we test to see if the diffusion coefficient in the low- W_0 micellar phase (the high-temperature phase above the lamellar phase) is an orientationally disordered version of the lamellar phase. If this were so, one would expect $D^{w,micellar} = 1/3 D_{\parallel}^{w,lamellar} + 2/3 D_{\perp}^{w,lamellar}$. This implies $D^{w,micellar} \geq 2/3 D_{\perp}^{w,lamellar}$. The water diffusion coefficient in the perpendicular-oriented lamellar phase is seen in Figure 9 to be larger than the extrapolation of the micellar temperature dependence to 298 K (of the Arrhenius temperature dependence using eq 18) from the micellar phase: $D^{w,micellar} \approx 0.82 D_{\perp}^{w,lamellar}$, a value that is consistent with the above argument.

The activation barrier for *surfactant diffusion* (obtained from the lower fitted slope in Figure 9) is $4646K \approx 39$ kJ/mol, that is, 1.8 times that of water diffusion. Soap diffusion in the perpendicular-oriented lamellar phase is not statistically different from the linear extrapolation of the Arrhenius temperature dependence in the micellar phase.

4. Estimates Relating Diffusion, Relaxation, and Structure

We relate our $C_{12}E_6$ diffusion measurements in the hexagonal and cubic phases to typical structure sizes based on correlation times deduced from plots in different phases of relaxation rate versus frequency.²⁰ Moreover, we use our results to elucidate the nature of the high- and low-water-content micellar phases.

(1) The hexagonal phase: The structure of the building block of the hexagonal phase was shown in section 3.3 to be consistent with surfactant cylinders (bare radius $r = 1.88$ nm and hydrated radius $R = 2.46$ nm). For the diffusion of a $C_{12}E_6$ molecule around the planar surface of a cylinder, the mean-squared distance diffused during the correlation time, τ_{cyl} (obtained from fits to the relaxation measurements in ref 20), is

$$\langle \mathcal{R}^2 \rangle = 4D\tau_{cyl} \quad (19)$$

If we use the measured diffusion coefficient $D_{\parallel}^{s,hexagonal} = 6.7 \times 10^{-12}$ m²/s at $W_0 = 30$ and the correlation time 29 ns obtained in ref 20, we calculate an effective radius of $\mathcal{R} = 0.9$ nm. It is unclear what cylinder radius one should use for the diffusion of a surfactant molecule, but it is reasonable that it should be less than the hydrated radius $R = 2.46$ nm.

(2) The cubic phase: The unit cell of the cubic phase sketched in Figure 6 is a cube of edge $a = 2\sqrt{2} \times 2r$,³⁴ where r is the cylinder radius. For $r \approx 1.88$ nm, we get $a = 10.6$ nm. This value is in good agreement with the value 11.8 nm from X-ray scattering.³⁵ The shortest distance (along a cylinder center) between contact points with other

cylinders is given by

$$L = \frac{\sqrt{3}}{4}a = 4.6 \text{ nm} \quad (20)$$

Alternatively, using the values $D = 3D^{\text{s.cubic}} = 2.8 \times 10^{-11} \text{ m}^2/\text{s}$ (Table 3) and $\tau_{\text{cubic}} = 2 \times 10^{-7} \text{ s}$ (ref 20) and the relation

$$L^2 = 2D\tau_{\text{cubic}} \quad (21)$$

we obtain $L = 3.4 \text{ nm}$, as compared with the value 4.6 nm obtained from eq 20.

(3) The high- W_0 micellar phase: As discussed at the end of section 3.5.1, $D^{\text{w.micellar}} \approx D^{\text{w.isotropic}}$, and the micellar phase across the hexagonal–micellar phase transition is indeed quantitatively consistent with an orientationally isotropic distribution of cylinders with the same surface-associated water fraction.

(4) The low- W_0 micellar phase: If the micellar phase were composed of inverse spherical micelles, then we would expect water diffusion to be the same as or less than the soap diffusion. At the lowest water concentrations, this is still not true. In the regime we probe ($0.4 < W_0 < 7$), water diffusion is 3–20 times faster. Since $D^{\text{w}}/D_0^{\text{w}} \approx 0.01$, the water is clearly something intermediate between bulk water and water contained in a restricted cavity.

We find satisfactory agreement between the correlation times that we calculate in the hexagonal and cubic phases with those calculated in ref 20, especially considering that the latter were obtained from many-parameter fits. Furthermore, we find diffusion coefficients in the high-water-content micellar phase to be quantitatively consistent with those calculated from diffusion anisotropy measurements in the hexagonal phase. Thus, this lends credence to our picture of these phases being composed of similar (cylindrical) building blocks. Finally, we find that water diffusion in the low- W_0 micellar phase is too fast to be consistent with the water being contained in small inverse micelles.

5. Discussion and Conclusions

We have measured diffusion coefficients of unaligned C_{12}E_6 /water samples at different concentrations spanning all observed phases in this system. Water diffusion exhibited an overall decrease from the bulk water value with decreasing water–soap molar ratio, W_0 , while soap diffusion increased toward the bulk soap value, both by roughly 1 order of magnitude. Proton NMR spectra in the hexagonal and lamellar phases displayed broad surfactant peaks, and diffusion measurements in these phases exhibited larger statistical error than in the NMR-isotropic cubic and micellar phases.

To relate diffusion coefficients and mesophase structure quantitatively, we created monodomain samples in the hexagonal and lamellar phases by slow cooling from the high-temperature micellar phase inside the 11.7 T magnet. The quadrupolar splittings gave qualitative information about the nature and homogeneity of the aligned samples. They also gave quantitative estimates of the order parameter (of the water O–D bond with respect to the surface normal of the mesophase structure): $S_{\text{OD}} \approx 0.004$ – 0.008 .

Flexible surfactant cylinders have previously been suggested as the building blocks of the high- W_0 micellar phase and the hexagonal phase.²⁰ Our measurements of diffusion anisotropy in the hexagonal phase (close to the hexagonal–micellar transition) of both the deuterated water and C_{12}E_6 components are quantitatively consistent

with a simple model (following refs 28 and 29) where the soap self-organizes into cylindrical rods and the water diffuses in the presence of these cylindrical obstacles with a fraction of water being associated with the obstacle surfaces. The *simplest* model, one of perfectly aligned cylinders, was not sufficient; it was necessary to allow for the fluctuation of cylinder orientation (or cylinder undulations), parametrized in the model by a nonzero β . The evidence for cylinder fluctuations is consistent with earlier relaxation rate measurements (ref 20) which could not be fit without a low-frequency divergence (as a function of frequency) corresponding to long-wavelength cylinder fluctuations.

Moreover, if the structure of the cylinders were unchanged from that at $W_0 = 30$, all water would be in the surface-associated water layer at $W_0 \approx f_{W_0=30} \times 30 = 15$, corresponding to a surfactant volume fraction of $\phi \approx 0.59$. The closest packing of cylinders in the hexagonal phase occurs at a packing fraction of 0.90. If we use the volume of the hydrated cylinders, then this closest packing would occur at $\phi = 0.90/(1 + xd/r)^2 \approx 0.53$, that is, before all the water is surface-associated and, indeed, close to the actual appearance of the cubic phase.

Past results suggest that the cubic phase belongs to the $Ia3d$ space group (has the structure of the cubic-gyroid phase). Since the value of the isotropic diffusion coefficient in the cubic phase is contiguous with the W_0 dependence in the hexagonal phase, we picture this phase as consisting of close-packed cylinders, as shown in Figure 6 (this is consistent with the $Ia3d$ space group). We are thus also able to use structure estimates in the hexagonal phase to obtain a distance between cylinder contact points in the cubic phase of $L \approx 3.4$ – 4.6 nm . We also obtain (directly from the cylinder radius) the cubic lattice parameter $a = 10.6 \text{ nm}$, within 10% of the value 11.8 nm obtained from X-ray scattering.³⁵ In addition, surfactant diffusion in the cubic phase ($D^{\text{s.cubic}} \approx D_0^{\text{s}}/3$) was consistent with the connecting-cylinder model envisaged for the cubic phase.

Observations in the high- W_0 micellar phase were consistent with the diffusion of fixed-size cylindrical micelles. In this phase, the diffusion coefficients, D^{w} , agreed to within 2% with the isotropic quantity, $D^{\text{w.isotropic}}$, calculated from the hexagonal phase anisotropic diffusion coefficients, $D_{\parallel}^{\text{w.hexagonal}}$ and $D_{\perp}^{\text{w.hexagonal}}$, measured in section 3.3. The water diffusion coefficient decreased with decreasing W_0 . Soap diffusion also *decreased* with decreasing W_0 . In fact, the water-to-soap diffusion coefficient ratio (Figure 3) in this phase remains constant as a function of W_0 . This contrasts with the *general trend* (Figure 2) where soap diffusion increases as one increases the surfactant concentration. For example, if micellar size were increasing with decreasing W_0 and we were measuring molecular diffusion within a micelle, the diffusion coefficient would increase.

Indeed, this seemingly anomalous behavior is reasonable if we consider that the obstruction effect is essentially an excluded volume effect and applies equally to water and micellar diffusion; that is, the micellar diffusion also is obstructed by the excluded volume of other micelles (here, we ignore differences in excluded volume as seen by centers of mass of a water molecule and a cylindrical micelle). This decrease, coupled with the quantitative agreement of micellar and hexagonal phase diffusion, is strong evidence for containment of the soap in constant-size cylindrical micelles, with the soap diffusion coefficient reflecting the diffusion of micellar objects. An increase in the surfactant diffusion coefficient is observed upon decreasing W_0 across the micellar–hexagonal phase

boundary: this signals the transition from micellar diffusion to molecular surfactant diffusion.

It is also very clear from this work that the low- W_0 micellar phase cannot be modeled as fixed-size inverse micelles. For fixed-size inverse micelles, water diffusion should not be faster than soap diffusion. Indeed, water diffusion in inverse micelles should decrease with increasing W_0 in just the same way as soap diffusion with decreasing W_0 in the high- W_0 micellar phase. However, the water-to-soap diffusion coefficient ratio is not constant in the low- W_0 micellar phase. The observed *increase* in D^w and decrease in D^s with W_0 is consistent with the water *not being contained* in inverse micelles.

The temperature dependence of the diffusion coefficients was measured in magnetically aligned samples as well as in the high-temperature (high- and low- W_0) micellar phase. We found that the temperature dependence was consistent with Arrhenius behavior with a water activation energy consistent with that of bulk free water. This implies that the activation barrier is not significantly affected by the large fraction of surface-associated water. Also, this suggests that the penetration of water through hydrocarbon cores, although possible, is likely not a dominant mode of water transport.

Diffusion in perpendicular-oriented lamellar phases exhibited surfactant diffusion much smaller than the bulk surfactant value; that is, $D_{\perp}^{s,\text{lamellar}}/D_0^s < 1$ at concentrations spanning the lamellar phase. Since a ratio of unity would be expected for the simplest picture of a defect-free and/or obstruction-free lamellar phase, these observations are consistent with the proposed existence^{2,20,36} of defects or obstructions.

However, despite all of the internal consistencies—relating diffusion anisotropy in the hexagonal phase, diffusion coefficients in the cubic and high- W_0 micellar phases, and pure surfactant diffusion—there is one

remaining anomaly. The diffusion coefficients D^w and D^s for the hexagonal powder would be expected to equal the isotropic values $D_{\text{isotropic}}^w$ and $D_{\text{isotropic}}^s$ calculated using eqs 15 and 16 from the anisotropic diffusion coefficients. In fact, they are $D^w = 0.75D_{\text{isotropic}}^w$ and $D^s = 1.8D_{\text{isotropic}}^s$. Thus, the dynamics of water in the powder sample is more complicated than simply an ensemble average over domains with different orientations. A picture of soap-rich domain boundaries is consistent with these results: the water motion is restricted at sub-micrometer domain boundaries, while the soap diffusion is enhanced. Note that the above results are independent of any partial orientation that results from proximity to the micellar phase, because the powder sample results (from section 3.3) quoted above were seen to have deuterium NMR powder patterns. This anomaly, perhaps related to sample-memory effects via slow domain-coarsening dynamics, likely also gives rise to the statistical variation in powder diffusion coefficients.

This work demonstrates that magnetically aligned samples sidestep issues relating to sample history and provide a quantitatively consistent characterization of diffusion in surfactant mesophases. The cubic phase, potentially useful in medical drug-delivery applications,¹⁷ can be better characterized with structural information obtained from diffusion measurements in the cubic, hexagonal, and micellar mesophases. Finally, our results show that diffusion anisotropy measurements in nonionic surfactant mesophases provide quantitative connections to simple geometric models of nanoscale structure.

Acknowledgment. We acknowledge the Natural Sciences and Engineering Research Council of Canada for financial support.

LA046962R